



HAL
open science

Low-temperature synthesis of GeTe nanoparticles

Marek Bouška, Yaraslava Milasheuskaya, Miroslav Šlouf, Petr Knotek, Stanislav Pechev, Lubomír Prokeš, Lukáš Pečinka, Josef Havel, Miroslav Novák, Roman Jambor, et al.

► **To cite this version:**

Marek Bouška, Yaraslava Milasheuskaya, Miroslav Šlouf, Petr Knotek, Stanislav Pechev, et al.. Low-temperature synthesis of GeTe nanoparticles. *Chemistry - A European Journal*, 2024, 30 (61), pp.e202402319. 10.1002/chem.202402319 . hal-04784022

HAL Id: hal-04784022

<https://hal.science/hal-04784022v1>

Submitted on 14 Nov 2024

HAL is a multi-disciplinary open access archive for the deposit and dissemination of scientific research documents, whether they are published or not. The documents may come from teaching and research institutions in France or abroad, or from public or private research centers.

L'archive ouverte pluridisciplinaire **HAL**, est destinée au dépôt et à la diffusion de documents scientifiques de niveau recherche, publiés ou non, émanant des établissements d'enseignement et de recherche français ou étrangers, des laboratoires publics ou privés.



Distributed under a Creative Commons Attribution - NonCommercial 4.0 International License



Low-Temperature Synthesis of GeTe Nanoparticles

Marek Bouška,^[a] Yaraslava Milasheuskaya,^[b] Miroslav Šlouf,^[c] Petr Knotek,^[b] Stanislav Pechev,^[d] Lubomír Prokeš,^[e] Lukáš Pečinka,^[e] Josef Havel,^[e] Miroslav Novák,^[g] Roman Jambor,^[b] and Petr Němec*^[a]

Nanoparticles can offer an alternative approach to fabricate phase-change materials. The chemical synthesis of GeTe nanoparticles using organometallic precursors exploits high-boiling solvents and relatively high temperatures (close or even above crystallization temperatures), as reported in the available literature. The aim of this work is the preparation of GeTe nanoparticles by a low-temperature synthetic method exploiting new organometallic precursors and common organic solvents. Indeed, different preparation methods and characterization of GeTe nanoparticles is discussed. The characterization of the prepared nanomaterial was performed on the basis of X-

ray diffraction, transmission electron microscopy, scanning electron microscopy with energy dispersive X-ray spectroscopy, laser ablation time-of-flight mass spectrometry, Raman scattering spectroscopy, and dynamic light scattering. The results show that the low-temperature synthetic route leads to amorphous GeTe nanoparticles. Exploited organometallic precursor is stabilised by neutral ligand which can be isolated after the reaction and repeatedly used for further reactions. Furthermore, GeTe nanoparticle size can be tuned by the conditions of the synthesis.

Introduction

Binary and ternary metal and semimetal chalcogenides have received increasing interest over the last decades. These materials are found in applications such as energy devices, fuel and solar cells, light-emitting diodes, Li-ion batteries, and thermoelectric devices. In case of thermoelectrics, GeTe-based materials are heavily studied to enhance their figure-of-merit and other properties. In detail, in comparison with typical

thermoelectric material such as Bi₂Te₃, GeTe-based thermoelectrics present high figure-of-merit >2.0 and an energy conversion efficiency beyond 10%.^[1]

GeTe-based materials exist in different forms: bulk materials (including single crystals), thin films, fibers, and nanoparticles (NPs). Bulk GeTe-based materials can be prepared by different methods such as solid-state reaction, melting spinning, ball milling mechanical alloying, Bridgman–Stockbarger single crystal growth, hot extrusion, etc.^[1] Chalcogenide-based thin films which are important for a number of applications including phase change memories, optical sensing, nonlinear optical applications etc. are fabricated using deposition methods such as pulsed laser deposition,^[2] sputtering,^[3] metal organic chemical vapour deposition,^[4] hot wire chemical vapour deposition^[5] or atomic layer deposition.^[6] Furthermore, step index and photonic crystal fibers, transparent from visible region up to the mid-infrared and presenting large nonlinear refractive index, can be made from chalcogenide glasses.^[2] It is worthy to note that the ternary Ge–Sb–Te materials became famous because of Ovshinsky's discovery as new class of materials that are capable of quickly and reversibly transforming between amorphous and crystalline phases.^[7] These reversible phase transitions can be induced by the electric field or light and have become the basis for optical recording applications.^[8] Later on, a quick and reversible phase transition was also observed for binary GeTe itself as reviewed recently.^[9] However, all mentioned techniques require sophisticated fabrication equipment. In addition to bulk, fiber or thin film forms of GeTe-based materials, they can also be prepared in the form of NPs through a solution process.^[10] Thus, the synthesis of well-defined GeTe NPs either in the amorphous or in the crystalline form seems to be rather important, especially when the presence of NPs with various diameters gives the possibility of controlling the dimensions of nanostructures of tellurium-based materials.^[11]

[a] M. Bouška, P. Němec

Department of Graphic Arts and Photophysics, Faculty of Chemical Technology, University of Pardubice, Studentská 573, 53210 Pardubice, Czech Republic
E-mail: petr.nemec@upce.cz

[b] Y. Milasheuskaya, P. Knotek, R. Jambor

Department of General and Inorganic Chemistry, Faculty of Chemical Technology, University of Pardubice, Studentská 573, 53210 Pardubice, Czech Republic

[c] M. Šlouf

Institute of Macromolecular Chemistry, Czech Academy of Sciences, Heyrovského nam. 2, 162 06 Prague 6, Czech Republic

[d] S. Pechev


Institut de Chimie de la Matière Condensée de Bordeaux – CNRS, 87, av. du Dr. Albert Schweitzer, 33608 Pessac Cedex, France


[e] L. Prokeš, L. Pečinka, J. Havel

Department of Chemistry, Faculty of Science, Masaryk University, Kotlářská 2, 61137 Brno, Czech Republic

[g] M. Novák

Institute of Chemistry and Technology of Macromolecular Materials, Faculty of Chemical Technology, University of Pardubice, Studentská 573, Pardubice 532 10, Czech Republic

 Supporting information for this article is available on the WWW under <https://doi.org/10.1002/chem.202402319>

 © 2024 The Author(s). Chemistry - A European Journal published by Wiley-VCH GmbH. This is an open access article under the terms of the Creative Commons Attribution License, which permits use, distribution and reproduction in any medium, provided the original work is properly cited.

Most of the solution synthetic routes are realized at relatively high temperatures and strongly depend on the reaction conditions. For example, the reaction of $R_3P\text{Te}$ (R is octyl) with GeI_2 at 180°C provided rhombohedral GeTe microcrystals,^[12] but similar starting materials provided amorphous GeTe NPs in the presence of R_3P , R_3PO , and dodecanethiol at 250°C .^[13] The reaction of $R_3P\text{Te}$ with $\text{Ge}[\text{N}(\text{SiMe}_3)_2]_2$ strongly depends on the temperature: amorphous GeTe NPs could be prepared at 170°C , while the temperature of 250°C provided rhombohedral GeTe NPs.^[14] Finally, amorphous GeTe NPs were prepared from GeCl_2 -dioxane and $\text{Te}(\text{SiEt}_3)_2$ at 150°C .^[15] Therefore, all above mentioned syntheses have to be carried out in high-boiling solvents such as dodecanethiol, hexadecylamine, octadecene or oleylamine.^[13–15] Moreover, all these approaches proceed close to the crystallization temperatures of bulk GeTe ($T_c = 180^\circ\text{C}$)^[16] or sputtered films of GeTe ($T_c = 170^\circ\text{C}$).^[17] However, Caldwell *et al.* reported that the crystallization temperatures for the GeTe NPs depends on the size and observed crystallization temperature of 350 and 400°C for 2.6 and 1.8 nm GeTe NPs, respectively.^[13]

Based on above-mentioned facts, the aim of this work was to prepare the GeTe NPs at temperatures significantly below the crystallization temperature in the common organic solvents. Such low-temperature solution-based synthetic routes could be an appropriate alternative low-cost method for generating dimensionally controlled GeTe nanomaterial. Indeed, in the present paper we report on the low-temperature synthesis of GeTe NPs using the organometallic precursor, tetrahydrofuran (THF) as solvent, and we discuss the influence of the temperature on the size of GeTe material. Finally, the GeTe NPs were characterised by X-ray diffraction, transmission electron microscopy, high-resolution scanning electron microscopy, scanning electron microscopy with energy dispersive X-ray spectroscopy, laser ablation time-of-flight mass spectrometry, Raman scattering spectroscopy, and dynamic light scattering.

Experimental sections

NMR spectroscopy. The NMR spectra for ^1H , $^{13}\text{C}\{^1\text{H}\}$, and $^{31}\text{P}\{^1\text{H}\}$ were obtained using a Bruker Avance 500 NMR spectrometer. Internal referencing based on residual protio-solvent signals was used for the ^1H and $^{13}\text{C}\{^1\text{H}\}$ spectra. External referencing with H_3PO_4 (85%) was utilized for the $^{31}\text{P}\{^1\text{H}\}$ NMR spectra.

X-ray diffraction analysis. X-ray Diffraction experiment was performed on a Malvern Panalytical X'Pert Pro MPD diffractometer, using Co radiation in reflection mode. Powder sample was withdrawn from its closed Ar-protected container, then put on a corundum diffractometer sample holder. 48 minutes diffraction pattern was collected within the $15^\circ \leq 2\theta \leq 80^\circ$ range.

Transmission electron microscopy (TEM). A small volume (2 μL) of the nanoparticles was dispersed in ethanol and dropped onto the standard TEM copper grid covered with electron transparent carbon film. After 2 min the excess of the solution was removed by touching the bottom of the grid by a thin strip of filtration paper in order to avoid oversaturation and nanoprecipitation during the drying process, then the specimens were left to dry completely, and after drying they were transferred to a TEM microscope (Tecnaï G2 Spirit Twin 12; FEI company, Czech Republic) and observed at

accelerating voltage of 120 kV. Standard bright field imaging (TEM/BF) was applied to observe the morphology of the particles, energy-dispersive analysis of X-rays (TEM/EDX) yielded the elemental composition, and selected area electron diffraction (TEM/SAED) was used to verify the crystalline structures. The experimental electron diffraction patterns were transformed to 1D-diffractograms (by means of ProcessDiffraction^[18]) and compared with theoretical X-ray diffraction patterns (calculated with freeware Python package EDIFF^[19]) of the expected crystalline structures of GeTe (the three known GeTe crystalline modifications – rhombic α -GeTe, cubic β -GeTe, and orthorhombic γ -GeTe^[20] – were obtained from Crystallography Open Database^[21]).

Scanning electron microscopy (SEM) with energy-dispersive X-ray (EDX) spectroscopy. SEM EDX was performed on TESCAN, VEGA 3, EasyProbe, Brno, Czech Republic. Standard uncertainties of the EDX measurements were ± 2 at.%. Typically, the EDX measurements were performed at 3 spots per sample and averaged.

High-resolution scanning electron microscopy (HR-SEM). HR-SEM image was obtained using a JSM-7500F (JEOL, Tokyo, Japan) microscope with the accelerating voltage of 15 and 20 kV.

Raman scattering spectroscopy and dynamic light scattering. Raman scattering spectra excited by a laser operating at the wavelength $\lambda = 785$ nm were measured with a Dimension P2 (Lambda Solution, USA). The Raman spectra were reduced according to the Gammon-Shuker equation.^[22] The hydrodynamic size of the particles D_H was analysed by the dynamic laser scattering DLS (90Plus/BI-MAS Analyzer, Brookhaven Instruments Corp., USA) operated at 660 nm with a light output of 35 mW. D_H values were measured for 30 s at 10 replications, and these data were statistically processed in the form of a histogram. Experimental details of both methods and sample preparation are given in Ref.^[23a,b]

Laser ablation (LA) time-of-flight mass spectrometry (TOF MS). Mass spectra were recorded on a MALDI-7090 mass spectrometer (Shimadzu Kratos Analytical, UK) using an Nd-YAG laser ($\lambda = 355$ nm). The laser energy was scaled in arbitrary units (a.u.) from 0 to 180. The irradiated spot size was 100 μm in diameter. For measurements with higher resolution AXIMA Resonance mass spectrometer (Shimadzu Kratos Analytical, UK) hybrid quadrupole ion-trap time-of-flight mass spectrometer was used. The instrument was equipped with a nitrogen pulsed laser ($\lambda = 337$ nm). Mass spectra were recorded in the 100–1500 m/z range. All measurements were performed in both positive and negative reflectron ion modes. External mass calibration in both ionization modes was performed using clusters of red phosphorus giving an accuracy better than ± 20 mDa. Computer modelling of the isotopic envelopes using Launchpad software (Kompact version 2.9.3, 2011) from Kratos Analytical Ltd. (Manchester, UK) was used to determine stoichiometry of the detected clusters. For LA TOF mass spectrometry, sample of GeTe was dispersed in 1 mL of THF. The suspension in THF was sonicated for 5 min before deposition on the target. A 1 μL sample of a suspension was deposited on a stainless-steel target and dried under an air stream at room temperature (RT). The target was then introduced into a mass spectrometer, and the measurements started once the pressure decreased below 10^{-5} Pa. First, mass calibration was carried out using red phosphorus as the standard (with mass error being less than ± 50 mDa for all measurements) and each mass spectrum was then accumulated from at least 10 shots using 500 profiles.

Chemicals. Te powder (30 mesh, purity 99.997%) was purchased from Sigma-Aldrich (Steinheim, Germany). For comparison, GeTe powder (purity 99.999%) was purchased from ThermoFisher (Kandel, Germany). Red phosphorus was bought from Riedel deHaën (Hannover, Germany), tetrahydrofuran and dichlorome-

thane were purchased Sigma-Aldrich (Steinheim, Germany). All solvents were dried using Pure Solv-Innovative Technology equipment. Deuterated solvents such as CDCl_3 was purchased from GenChem, heated with solvent-appropriate drying agents, distilled under an argon atmosphere, degassed, and stored over molecular sieves. Starting materials such as diisopropyl phosphine oxide, Palladium(II) acetate, 1,1-bis(diphenylphosphino)ferrocene, triethylamine, Germanium(II) chloride dioxane complex (1:1) ($\text{GeCl}_2(\text{dioxane})$), silver trifluoromethanesulfonate (AgOTf), lithium triethyl borohydride (1 M solution in THF) were purchased from Sigma Aldrich and used as received.

Results and Discussion

Synthesis of GeTe Nanoparticles

All air-sensitive and moist operations were performed under an inert atmosphere using the standard Schlenk technique. The *N,N*-chelating ligand **L** (**L** is $[2-[(\text{Me})\text{C}=\text{N}(\text{C}_6\text{H}_3-2,6\text{-iPr}_2)]-6-[(\text{iPrO})_2\text{P}=\text{O}]\text{C}_5\text{H}_3\text{N}]$)^[24] was used to stabilise the initial ionic Ge-based complex $[\text{LGeCl}]^+ [\text{OTf}]^-$ (**1**) (Scheme 1; more details are given in SI).

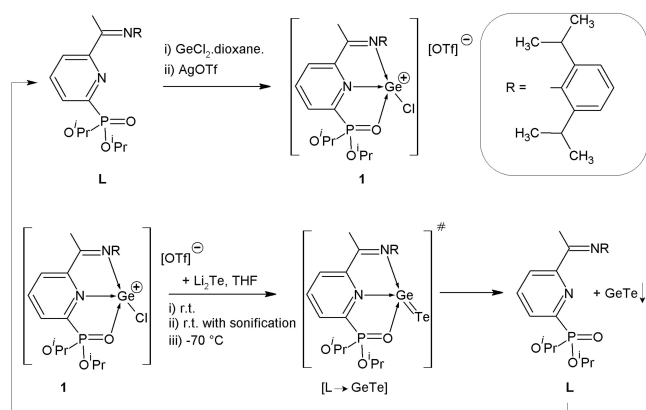
Compound **1** is soluble in polar organic solvents such as THF or CH_2Cl_2 , but almost insoluble in toluene and hexane. Compound **1** was characterised by NMR spectroscopy (complete NMR details are shown in SI; for NMR spectra, see Figures S1–S4 in SI). The $^31\text{P}\{^1\text{H}\}$ NMR spectrum of **1** revealed singlet resonance at δ 12.7 ppm, which is shifted downfield as compared to the value found for the starting ligand **L** (δ 7.2 ppm).^[24] This downfield shift is a clear proof of the $\text{P}=\text{O}\rightarrow\text{Ge}$ interaction in **1**. The presence of the OTf anion in **1** was confirmed by the quartet signal in $^{13}\text{C}\{^1\text{H}\}$ NMR at δ 119.5 ppm flanked with $^1J(^{19}\text{F}, ^{13}\text{C})=319.4$ Hz due to the presence of the CF_3 group. Finally, the ^1H NMR spectrum of **1** showed the singlet resonance at δ 2.57 ppm of $(\text{CH}_3)\text{C}=\text{N}$ being shifted downfield compared to the free ligand **L** (δ 2.25 ppm). This downfield shift proves the existence of the $\text{C}=\text{N}\rightarrow\text{Ge}$ interaction in **1**.

Complex **1** was tested as a suitable precursor for further synthesis of GeTe NPs. Therefore, the reaction of **1** with

suspension Li_2Te , prepared *in situ*, was tested (Scheme 1, for details – SI). Li_2Te was added dropwise via a cannula to the THF solution of **1** at RT and stirred for 24 hours. The resulting suspension was filtered and the solid material was washed with THF. Subsequently, this solid was redispersed in THF, the suspension was sonicated (FisherBrand FB15053H ultrasonic bath, 560 W (Fisher Scientific, UK)) for 10 minutes and the particle size of this solid material was characterised by dynamic light scattering (DLS). The histogram of the hydrodynamic size (D_H) was bimodal, formed from the signal of the primary particles and further from their agglomerates. Primary GeTe particles ($D_H=60$ nm, Figure 1 – black curve) were agglomerated to the highly populated particles GeTe with $D_H=700$ nm, i.e. the mean D_H increased to the 550 nm, similar to other systems of metals^[23a,25], oxides^[23b,26] or layered perovskites^[27] in the environment out of distilled water.^[28]

Therefore, the reaction conditions were modified and the Li_2Te suspension was added to the sonicated THF solution of **1** at RT. The reaction was subsequently sonicated for an additional 10 minutes. The short time of sonication was chosen because it is well known that a longer time of sonication led to the disappearance of nanoparticles and promoted re-agglomeration.^[23a,29,30] Further procedures were similar as described in the previous case. The histogram of D_H for solid GeTe prepared by this method was again bimodal (Figure 1 - blue curve), with maximums at 115 nm and agglomerates GeTe at 255 nm. Thus, sonication did not allow isolation of nano-GeTe particles either. Finally, the influence of temperature was investigated. Thus, the Li_2Te suspension was added dropwise to the THF solution of **1** at -50°C , the solution was stirred for an additional 4 h at this temperature and warmed to RT. Further procedures were similar as described previously. The histogram of D_H for solid GeTe prepared by this low-temperature method revealed that the hydrodynamic diameter of the primary particles was 71 nm (Figure 1 – red curve).

We suppose that the reaction of **1** with Li_2Te produced an unstable complex $[\text{L}\rightarrow\text{GeTe}]$ that decomposes into the GeTe material together with the free ligand **L**. However, the low temperature slows down this decomposition and provides the GeTe NPs. The presence of ligand **L** was always detected in the



Scheme 1. Preparation of GeTe NPs via the complex $[\text{LGeCl}]^+ [\text{OTf}]^-$ (**1**).

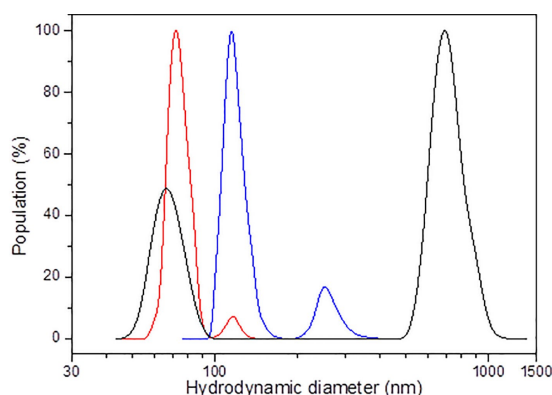


Figure 1. Histograms of the hydrodynamic diameter for GeTe particles redispersed in THF and sonicated for 10 min: synthesis at RT (black); synthesis at RT together with ultrasonication (blue); synthesis at -50°C (red).

reaction mixture after the addition of Li_2Te . Additionally, after the isolation of GeTe NPs, we were able to use the filtrated THF solution containing the ligand L, for the synthesis of another batch of 1 and GeTe NPs. This low-temperature procedure was repeated three times, and prepared GeTe NPs were characterised by other techniques.

Characterisation of GeTe Nanoparticles

The prepared GeTe nanoparticles were further characterised by TEM, SEM EDX, HR-SEM, Raman scattering spectroscopy, XRD, and LA TOF mass spectrometry. At room temperature, the powder XRD patterns exemplified in Figure 2 show two very broad halos and no diffraction peaks, which demonstrates an amorphous material.

TEM characterisation of the prepared GeTe nanoparticles is summarised in Figure 3. Bright field imaging (TEM/BF; Figure 3a) showed that the particles were isometric, rounded, without sharp crystal facets, and of average size ca 20 nm. The

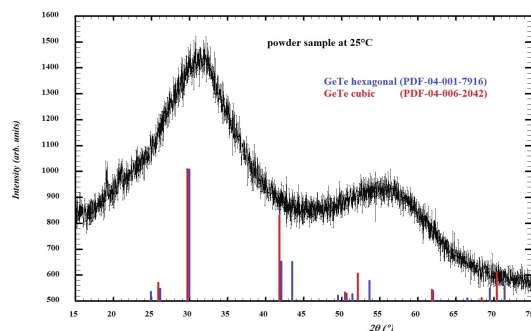


Figure 2. Room temperature powder X-ray diffraction ($\text{CoK}\alpha$ $\lambda = 1.790$ Å) pattern of GeTe sample. Blue and red lines correspond to X-ray diffraction pattern of low temperature hexagonal (rhombohedral) GeTe and high temperature cubic GeTe phase, respectively. Data were used from the database Powder Diffraction File PDF-4 + 2023.

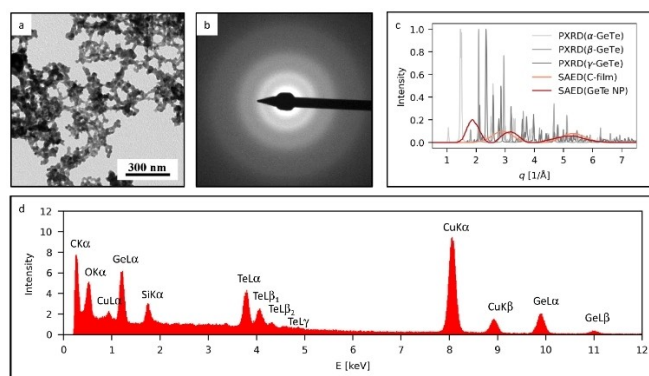


Figure 3. TEM analysis of GeTe nanoparticles: (a) TEM/BF – bright field image showing the morphology of the nanoparticles, (b) TEM/SAED – 2D-electron diffraction pattern, (c) comparison of experimentally determined 1D-electron diffraction pattern (dark red line) with control sample containing only the supporting carbon film (light red line) and d) 1D-powder X-ray diffraction patterns of α -GeTe (light grey), β -GeTe (medium grey), γ -GeTe (dark grey line), and (d) TEM/EDX – energy-dispersive analysis of X-rays showing elemental composition of the nanoparticles.

experimental electron diffraction pattern (TEM/SAED; Figure 3b) did not display any sharp peaks, which documented that the particles were amorphous. This observation was consistent with the XRD results. Two of the three observed broad diffraction maxima of the analysed GeTe nanoparticles roughly corresponded to the amorphous carbon supporting film (compare light red and dark red lines in Figure 3c). The highest diffraction maximum of GeTe nanoparticles, observed at ~ 2 Å, indicated certain periodicity in otherwise amorphous material. The fact that the observed particles were an amorphous form of GeTe^[20] was confirmed by energy dispersive spectroscopy (Figure 3d). The EDX spectrum was dominated by the strong peaks of Cu and C (signal from the supporting carbon coated copper grid as the nanoparticles were quite small) and peaks of Ge and Te (confirmation of the NPs elemental composition). The peak of oxygen (at $E = 0.52$ keV) suggested a certain oxidation of the nanoparticles. The peak of silicon could be attributed to the fluorescence from Si-detector.^[31]

The SEM EDX results (shown in SI as Figure 5) suggested that the composition (atomic percentages) of the resulting nanoparticles is $\text{Ge}_{48}\text{Te}_{52}$ (± 2 at.%). The distribution of elements was clarified by the EDX results, which showed that the germanium and tellurium elements were homogeneously distributed in the whole sample. The samples were further analysed by HR-SEM. The samples for this analysis were prepared by the deposition of GeTe dispersion in THF on the brass sample holder. After the evaporation of THF, samples were coated with 15 nm of a gold conductive layer and SEM scans were acquired at 15 kV of acceleration voltage. Two different concentrations of GeTe in THF (5 mg/ml and 0.5 mg/ml) were chosen to study the dependence of the concentration on the size and formation of the agglomerates of the prepared GeTe particles. This study showed that for a concentration of 5 mg/ml, only GeTe agglomerates were formed (Figure 4A). However, even in these agglomerates, particles can be found with a size of approximately 136 nm (Figure 4A). However, a decrease in concentration to 0.5 mg/ml led to the formation of well-separated GeTe particles with a particle size of approximately 155 nm (Figure 4B).

The Raman spectra (exemplified in Figure 5) for both synthesised GeTe materials (synthesised at RT and -50 °C) were within experimental error identical, e.g. the temperature of the synthesis effect mainly the size of the agglomerates, not the local structure itself. The most intensive bands in the Raman spectra are attributed to the vibrations in bending mode (90 cm^{-1} : overlapping peaks assigned to the $\nu_4(\text{F}_2)$ and $\nu_2(\text{E})$), symmetric stretching modes (120 and 159 cm^{-1} : A_1 motion of the corner and edge-sharing tetrahedra) and antisymmetric stretching mode (221 cm^{-1} : $\nu_3(\text{F}_2)$) of the $\text{GeTe}_{4-n}\text{Ge}_n$ tetrahedra, Figure 4.^[32a,b] The population of the different tetrahedra $\text{GeTe}_{4-n}\text{Te}_n$ was calculated in according to the Phillip's model^[32c,d] for GeTe composition such as 6.25% GeTe_4 , 25% GeTe_3Ge , 37.5% GeTe_2Ge_2 , 25% GeTeGe_3 and 6.25% GeGe_4 . The low intensive band at 307 cm^{-1} could be thus associated with the presence of the Ge–Ge homopolar bond with the population ca. 6–10% in the GeTe structure.^[33] The possible presence of the Te–Te stretching mode should be detectable at the 150 cm^{-1} ,

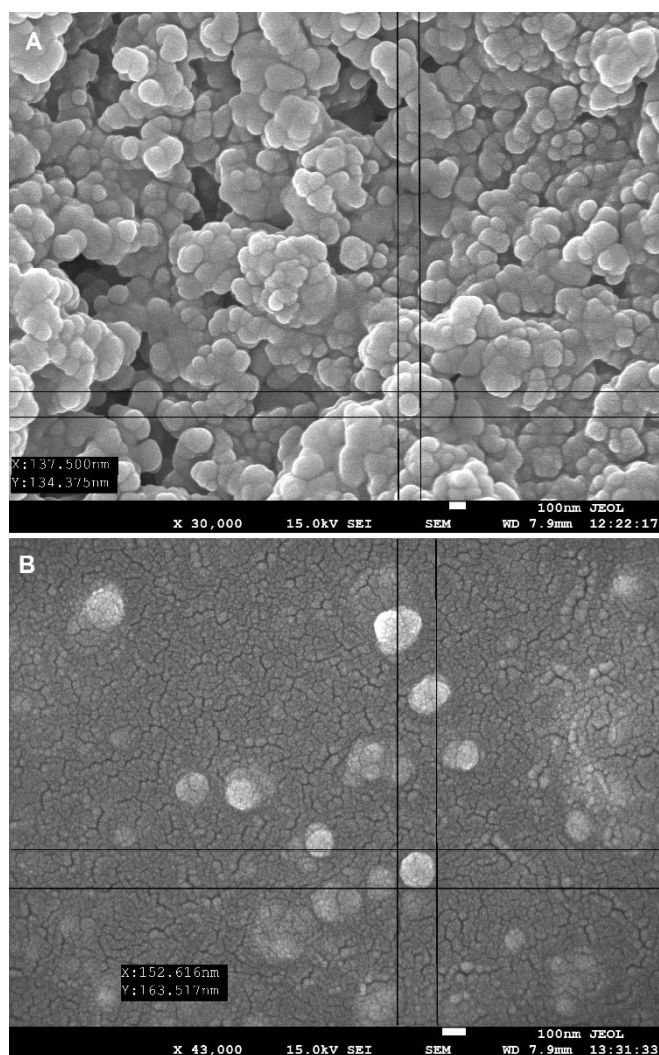


Figure 4. A) HR-SEM image of GeTe NPs (prepared from THF suspension, 5 mg/ml). B) HR-SEM image of GeTe NPs (prepared from THF suspension, 0.5 mg/ml).

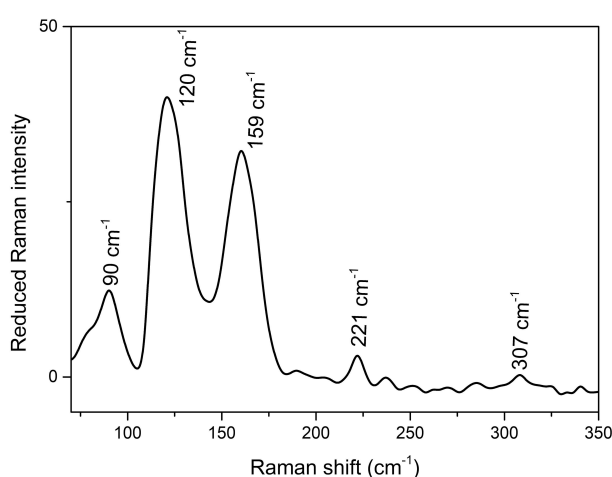


Figure 5. Raman spectrum of GeTe powder synthesised at $-50\text{ }^{\circ}\text{C}$.

^[34a,b] but it is overlapped by the more intensive bands of A_1 mode of the edge-sharing tetrahedra.

The Raman spectra are qualitatively comparable with the spectra of the thin films of amorphous GeTe material prepared by magnetron sputtering^[35,36] or PLD techniques.^[32b] When the GeTe is in the form of nanowires^[37] or in the form of thin film prepared by CVD from organometallic precursors,^[38] the ratio of signals representing edge/corner shared GeTe_4 tetrahedra strongly decreases to about 1:5, which corresponds to the structural preference of the corner-shared arrangement. In the Raman spectra of the crystalline form of GeTe there is a significant amplification and decrease in the bandwidth of the signal at 90 cm^{-1} ^[32b,c,39] due to the high Raman activity of the rhombohedrally deformed rock-salt structure.

The LA TOF MS data of the synthesised GeTe material, commercial Te, and commercial GeTe are shown in Figure 5. It can be seen that ion clusters of binary GeTe were well detected on the newly synthesised material. Only a binary cluster GeTe_2^+ was detected in commercial material, indicating the most stable ion formed in the gas phase. In addition to Te_n^- clusters ($n=1-5$), series of GeTe_n^- ($n=2-4$), GeTe_nOH^- ($n=1-3$), and $\text{GeTe}_n\text{O}_2\text{H}^-$ ($n=1-4$) clusters were detected in synthesised materials. Several signals of contaminants from synthesis and/or from solvents were observed, however they do not complicate data evaluation (marked with asterisk in Figure 6).

Some new signals corresponding to Ge_mTe_n^- were detected when mass spectrometer equipped with quadrupole ion trap (Axima Resonance) was used (Figure S6). The newly observed signals of Ge_mTe_n^- clusters were identified as those with the number of Ge atoms: $m=2-6$ and number of Te atoms $n=1-3$.

Experimentally recorded mass spectra were compared with theoretical ones. Comparison for m/z region 470–640 Da is given as Figure S7. Identification shows clear agreement between exact masses of given isotopes and the intensity ratio of isotopes matches nicely with the theoretical ones.

Synthesis of Materials with GeTe NPs

The low-temperature synthetic method of GeTe NPs *via* the decomposition of $[\text{L} \rightarrow \text{GeTe}]$ also allows the very efficient combination of GeTe NPs with other substrates. We repeated

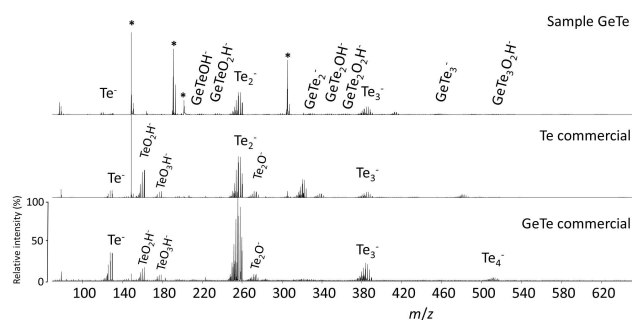


Figure 6. Comparison of the mass spectra of GeTe synthesised material, commercial Te, and commercial GeTe in the 70–650 m/z region in the negative ion mode. Asterisk (*) indicates m/z values corresponding to contamination.

the synthesis of GeTe NPs in THF at -50°C and in this solution single wall carbon nanotubes (SWCNTs) in weight ratio GeTe:SWCNT = 1:1 and 5:1 were added. The reaction mixtures were warmed at RT and the prepared material was characterised by EDX and HR-SEM. EDX measurement confirmed the presence of Ge and Te atoms in the samples. HR-SEM scans of the GeTe:SWCNTs samples with two studied weight ratios showed a different distribution of GeTe particles within the SWCNTs matrix. The formulation with the weight ratio of GeTe:SWCNTs = 1:1 revealed the formation of only GeTe agglomerates with nonuniform incorporation into the matrix of SWCNTs. This led to the observation of GeTe-rich and GeTe-poor regions (Figure 7A). On the contrary, a more homogeneous distribution of GeTe agglomerates was found in samples with a weight ratio of 5:1 (Figure 7B). It is worth noting that the GeTe agglomerates in this sample are composed of particles with a size of approximately 35 nm, therefore a clear influence of the presence of SWCNTs on the size of the GeTe particles is found.

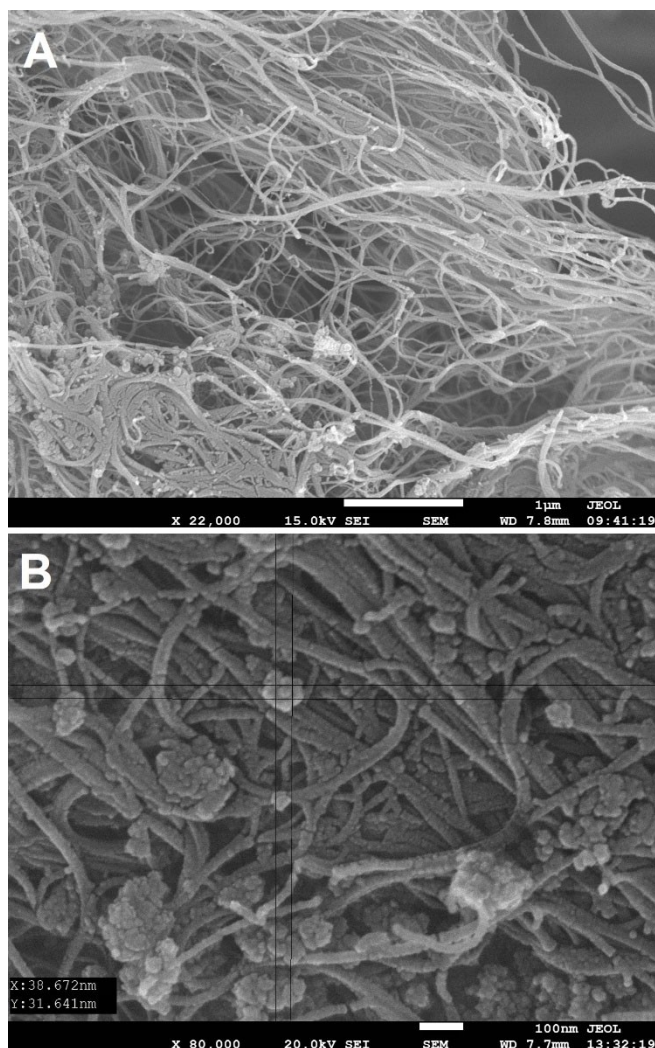


Figure 7. A) HR-SEM image of GeTe NPs with SWCNTs (prepared from THF solution, weight ratio 1:1), B) HR-SEM image of GeTe NPs with SWCNTs (prepared from THF solution, weight ratio 5:1).

Conclusions

Amorphous GeTe nanoparticles were prepared by the original low-temperature synthetic method employing a new organometallic precursor stabilised by neutral ligand L which can be isolated after the reaction and used for further reactions. Modification of reaction conditions such as temperature, sonication, or time led to preparation of different sizes of nanoparticles, which were evaluated by DLS measurements. The XRD patterns of GeTe nanoparticles confirmed that they are of an amorphous nature. SEM EDX suggested that the composition of the resulting nanoparticles is $\text{Ge}_{48}\text{Te}_{52}$ (± 2 at.%). HR-SEM of GeTe NPs showed homogeneity of the diameter of the nanoparticles. TEM showed that the particles were isometric, rounded, without sharp crystal facets, and averaged ~ 20 nm in size. The experimental electron diffraction pattern did not display sharp peaks, which again documented that the particles were amorphous. Raman scattering spectroscopy gave insight into the local structure of the prepared nanoparticles. LA TOF mass spectra of GeTe nanoparticles contain Te_n^- clusters ($n=1-5$), GeTe_n^- ($n=2-4$) and Ge_mTe_n^- ($m=2-6$, $n=1-3$) species and some clusters contaminated by oxygen and hydrogen. In conclusion, a low-temperature synthetic method using neutral ligands can be an effective route for the preparation of chalcogenide-based materials in the form of amorphous nanoparticles. Finally, the easy low-temperature synthetic method of GeTe NPs allows for a very efficient way to combine GeTe NPs with different substrates. In future work, we plan to deposit GeTe NPs in a form of thin films with the outlook of measurement of their thermoelectric performance or other applications.

Acknowledgements

The financial support of the Czech Science Foundation under the project No. 22-07635S is greatly acknowledged. Open Access publishing facilitated by Univerzita Pardubice, as part of the Wiley - CzechELib agreement.

Conflict of Interests

The authors declare no conflict of interest.

Data Availability Statement

The data that support the findings of this study are available from the corresponding author upon reasonable request.

Keywords: Nanoparticles · Chalcogenides · GeTe · Organometallic precursor

- [1] a) M.-R. Gao, Y.-F. Xu, J. Jiang, S.-H. Yu, *Chem. Soc. Rev.* **2013**, *42*, 2986–3017; b) Q. Sun, M. Li, X.-L. Shi, S.-D. Xu, W.-D. Liu, M. Hong, W. Lyu, Y. Yin, M. Dargusch, J. Zou, Z.-G. Chen, *Adv. Energy Mater.* **2021**, *11*, 2100544; c) M. Hong, M. Li, Y. Wang, X.-L. Shi, Z.-G. Chen, *Adv. Mater.*

- 2023, 35, 2208272; d) L.-C. Yin, W.-D. Liu, M. Li, D.-Z. Wang, H. Wu, Y. Wang, L. Zhang, X.-L. Shi, Q. Liu, Z.-G. Chen, *Adv. Funct. Mater.* **2023**, 33, 2301750; e) L.-C. Yin, W.-D. Liu, M. Li, Q. Sun, H. Gao, D.-Z. Wang, H. Wu, Y.-F. Wang, X.-L. Shi, Q. Liu, Z.-G. Chen, *Adv. Energy Mater.* **2021**, 11, 2102913; f) D.-Z. Wang, W.-D. Liu, Y. Mao, S. Li, L.-C. Yin, H. Wu, M. Li, Y. Wang, X.-L. Shi, X. Yang, Q. Liu, Z.-G. Chen, *J. Am. Chem. Soc.* **2024**, 146, 1681–1689; g) W.-D. Liu, L.-C. Yin, L. Li, Q. Yang, M. Li, X.-L. Shi, Q. Liu, Y. Bai, I. Gentle, L. Wang, Z.-G. Chen, *Energy Environ. Sci.* **2023**, 16, 5123–5135.
- [2] a) P. Němec, J. Přikryl, V. Nazabal, M. Frumar, *J. Appl. Phys.* **2011**, 109, 073520; b) P. Němec, V. Takats, A. Csik, S. Kokenyesi, *J. Non-Cryst. Solids* **2008**, 354, 5421–5424; c) P. Němec, V. Nazabal, A. Moreac, J. Gutwirth, L. Beneš, M. Frumar, *Mater. Chem. Phys.* **2012**, 136, 935–941; d) M. Bouška, S. Pechev, Q. Simon, R. Boidin, V. Nazabal, J. Gutwirth, E. Baudet, P. Němec, *Sci. Rep.* **2016**, 6, 26552; e) J. D. Musgraves, J. Hu, L. Calvez, in *Springer Handbook of Glass*, Springer, Switzerland **2019**, ISBN9783319937267.
- [3] a) N. Daichakomphu, S. Abbas, T.-L. Chou, L.-Ch Chen, K.-H. Chen, A. Sakulkalavek, R. Sakdanuphab, *J. Alloy. Compound.* **2022**, 893, 162342; b) Y. Zhao, L. Tang, S. Yang, S. P. Lau, K. S. Teng, *Nanoscale Res. Lett.* **2020**, 15, 138; c) J.-W. Park, S. H. Baek, T. D. Kang, H. Lee, Y.-S. Kang, T.-Y. Lee, D.-S. Suh, K. J. Kim, Ch. K. Kim, Y. H. Khang, J. L. F. Da Silva, S.-H. Wei, *Appl. Phys. Lett.* **2008**, 93, 021914; d) B.-S. Lee, J. R. Abelson, S. G. Bishop, D.-H. Kang, B. Cheong, K.-B. Kim, *J. Appl. Phys.* **2005**, 97, 093509; e) M. Bouška, V. Nazabal, J. Gutwirth, T. Halenkovič, J. Přikryl, S. Normani, P. Němec, *Opt. Lett.* **2020**, 45, 1067–1070; f) T. Halenkovič, M. Baillieul, J. Gutwirth, P. Němec, V. Nazabal, *J. Mater.* **2022**, 8, 1009–1019; g) M. Bouška, V. Nazabal, J. Gutwirth, T. Halenkovič, P. Němec, *J. Non-Cryst. Solids* **2021**, 569, 121003.
- [4] a) R.-Y. Kim, H.-G. Kim, S.-G. Yoon, *Appl. Phys. Lett.* **2006**, 89, 102107; b) B. J. Choi, S. Choi, Y. C. Shin, C. S. Hwang, J. W. Lee, J. Jeong, Y. J. Kim, S.-Y. Hwang, S. K. Hong, *J. Electrochem. Soc.* **2007**, 154, H318; c) G. S. Tompa, S. Sun, C. E. Rice, J. Cuchiaro, E. Dons, *Mater. Res. Soc. Symp. Proc.* **2007**, 997, 110–08.
- [5] A. Abrutis, V. Plausinaitiene, M. Skapas, C. Wiemer, O. Salicio, A. Pirovano, E. Varesi, S. Rushworth, W. Gawelda, J. Siegel, *Chem. Mater.* **2008**, 20, 3557–3559.
- [6] a) C. S. Hwang, Y. J. Kim, Y. J. Son, S. K. Hong, *Chem. Mater.* **2007**, 19, 4387–4389; b) J. Lee, S. Choi, C. Lee, Y. Kang, D. Kim, *Appl. Surf. Sci.* **2007**, 253, 3969.
- [7] S. R. Ovshinsky, *Phys. Rev. Lett.* **1968**, 21, 1450–1453.
- [8] a) N. Yamada, *Phys. Status Solidi B-Basic Solid State Phys.* **2012**, 249, 1837–1842; b) I. Friedrich, V. Weidenhof, W. Njoroge, P. Franz, M. Wuttig, *J. Appl. Phys.* **2000**, 87, 4130–4134; c) M. Wuttig, D. Lüsebrink, D. Wamwangi, W. Welnic, M. Gilleßen, R. Dronskowski, *Nat. Mater.* **2007**, 6, 122–127.
- [9] K. Singh, S. Kumari, H. Singh, N. Bala, P. Singh, A. Kumar, A. Thakur, *Appl. Nanosci.* **2023**, 13, 95–110.
- [10] B. J. Kooi, M. Wuttig, *Adv. Mater.* **2020**, 32, 1908302.
- [11] S. Atherton, B. Steele, S. Sasaki, *Crystals* **2017**, 7, 78.
- [12] M. R. Buck, I. T. Sines, R. E. Schaak, *Chem. Mater.* **2010**, 22, 3236–3240.
- [13] M. A. Caldwell, S. Raoux, R. Y. Wang, H. S. P. Wong, D. J. Milliron, *J. Mater. Chem.* **2010**, 20, 1285–1291.
- [14] I. U. Arachchige, R. Soriano, Ch. D. Malliakas, S. A. Ivanov, M. G. Kanatzidis, *Adv. Funct. Mater.* **2011**, 21, 2737–2743.
- [15] S. Schulz, S. Heimann, K. Kaiser, O. Prymak, W. Assenmacher, J. T. Brüggemann, B. Mallick, A.-V. Mudring, *Inorg. Chem.* **2013**, 52, 14326–14333.
- [16] M. Libera, M. Chen, *J. Appl. Phys.* **1993**, 73, 2272.
- [17] M. Chen, K. A. Rubin, R. W. Barton, *Appl. Phys. Lett.* **1986**, 49, 502–504.
- [18] J. L. Labar, *Ultramicroscopy* **2005**, 103, 237–249.
- [19] <https://pympi.org/project/ediff>.
- [20] A.-K. U. Michel, F. Donat, A. Siegfried, O. Yarema, H. Fang, M. Yarema, V. Wood, Ch. R. Müller, D. J. Norris, *J. Appl. Phys.* **2021**, 129, 095102.
- [21] S. Grazulis, D. Chateigner, R. T. Downs, A. T. Yokochi, M. Quiros, L. Lutterotti, E. Manakova, J. Butkus, P. Moeck, A. Le Bail, *J. Appl. Crystallogr.* **2009**, 42, 726–729.
- [22] R. Shuker, W. R. Gammon, *Phys. Rev. Lett.* **1970**, 25, 222.
- [23] a) J. Opršal, L. Bláha, M. Pouzar, P. Knotek, M. Vlček, K. Hrdá, *Environ. Sci. Pollut. Res. Int.* **2015**, 22, 19124–19132; b) T. Řičica, L. Dostál, Z. Ružičková, L. Beneš, P. Němec, M. Bouška, J. Macák, P. Knotek, P. Ruleová, R. Jambor, *Chem. A Eur. J.* **2018**, 24, 14470–14476.
- [24] M. Novák, J. Turek, Y. Milasheuskaya, M. Syková, L. Dostál, J. Stalmans, Z. Ružičková, K. Jurkschat, R. Jambor, *Dalton Trans.* **2023**, 52, 2749–2761.
- [25] M. Srb, Y. Milasheuskava, R. Jambor, K. Kopecká, P. Knotek, *ChemistrySelect* **2021**, 6, 3926–3931.
- [26] a) J. Báčova, P. Knotek, K. Kopecká, L. Hromádko, J. Čapek, P. Nývltová, L. Brůčková, L. Schroterová, B. Šestáková, J. Palarčík, M. Motola, D. Čížková, A. Bezrouk, J. Handl, Z. Fiala, E. Rudolf, Z. Bílková, J. M. Macák, T. Roušar, *Int. J. Nanomed.* **2022**, 17, 4211–4225; b) M. A. Al-Khafaji, A. Gaál, A. Wacha, A. Bota, Z. Varga, *Materials* **2020**, 13, 3101.
- [27] H. Gao, S. Shori, X. Chen, H.-C. Zur Loye, H. J. Ploehn, *J. Colloid Interface Sci.* **2013**, 392, 226–236.
- [28] M. Sedlák, *J. Phys. Chem. B* **2006**, 110, 4329–4338.
- [29] I. Kaur, L.-J. Ellis, I. Romer, R. Tantra, M. Carriere, S. Allard, M. Mayne-L'Hermitte, C. Minelli, W. Unger, A. Potthoff, S. Rades, E. Valsami-Jones, *J. Vis. Exp.* **2017**, 130, e56074.
- [30] A. L. Poli, T. Batista, C. C. Schmitt, F. Gessner, M. G. Neumann, *J. Colloid Interface Sci.* **2008**, 325, 386–390.
- [31] D. B. Williams, C. B. Carter, *Transmission Electron Microscopy*, 2nd ed. Springer, New York **2009**, ISBN 978-0387765006.
- [32] a) W. Lan, L. Cao, Y. Fu, J. Fang, J. Zhang, J. Wang, *Vacuum* **2022**, 197, 110847; b) P. Němec, V. Nazabal, A. Moreac, J. Gutwirth, L. Beneš, M. Frumar, *Mater. Chem. Phys.* **2012**, 136, 935–941; c) K. S. Andrikopoulos, S. N. Yannopoulos, G. A. Voyiatzis, A. V. Kolobov, M. Ribes, J. Tominaga, *J. Phys. Condens. Matter* **2006**, 18, 965–979; d) O. Salicio, C. Wiemer, M. Fanciulli, W. Gawelda, J. Siegel, C. N. Afonso, V. Plausinaitiene, A. Abrutis, *J. Appl. Phys.* **2009**, 105, 033520.
- [33] J. Y. Raty, W. Zhang, J. Luckas, C. Chen, R. Mazzarello, C. Bichara, M. Wuttig, *Nat. Commun.* **2015**, 6, 7467.
- [34] a) J. Tominaga, N. Atoda, *Jpn. J. Appl. Phys.* **1999**, 38, L322–L323; b) B. Liu, Z. T. Song, T. Zhang, S. L. Feng, B. M. Chen, *Chin. Phys.* **2004**, 13(11), 1947–1950.
- [35] K. S. Andrikopoulos, S. N. Yannopoulos, A. V. Kolobov, P. Fons, J. Tominaga, *J. Phys. Chem. Solids* **2015**, 68, 1074–1078.
- [36] A. Ali, S. M. Ansari, B. Ehab, B. Mohammad, D. H. Anjum, H. M. Aldosari, *Mater. Res. Bull.* **2022**, 146, 111575.
- [37] S. Park, T. Kim, S. Hwang, D. Park, M. Ahnac, M.-H. Cho, *J. Mater. Chem. C* **2022**, 8(32), 11032–11041.
- [38] S. L. Hawken, R. Huang, C. K. de Groot, A. L. Hector, M. Jura, W. Levason, G. Reid, G. B. Stenning, *Dalton Trans.* **2019**, 48(1), 117–124.
- [39] G. Kalra, S. Murugavel, *AIP Adv.* **2015**, 5, 047127.

Manuscript received: June 17, 2024
Accepted manuscript online: August 19, 2024
Version of record online: October 16, 2024